Available online at www.sciencedirect.com

SciVerse ScienceDirect

Acta Materialia 60 (2012) 2568–2577

Acta MATERIALIA

www.elsevier.com/locate/actamat

In situ synchrotron tomographic investigation of the solidification of an AlMg4.7Si8 alloy

D. Tolnai [a,b,*], P. Townsend [a,1], G. Requena [a], L. Salvo [c], J. Lendvai [b], H.P. Degischer [a]

[a] Institute of Materials Science and Technology, Vienna University of Technology, Karlsplatz 13/308, A-1040 Vienna, Austria
[b] Eötvös Loránd University, Department of Materials Physics, POB 32, H-1518 Budapest, Hungary
[c] Université de Grenoble, SIMaP/GPM2, UMR CNRS 5266, UJF, BP46, F-38402 Saint-Martin d'Hères Cedex, France

Received 13 October 2011; received in revised form 19 December 2011; accepted 14 January 2012
Available online 2 March 2012

Abstract

The solidification sequence of an AlMg4.7Si8 alloy is imaged in situ by synchrotron microtomography. Tomograms with $(1.4\ \mu m)^3$/voxel have been recorded every minute while cooling the melt from 600 °C at a cooling rate of 5 K min^{-1} to 540 °C in the solid state. The solidification process starts with the three-dimensional evolution of the α-Al dendritic structure at 590 °C. The growth of the α-Al dendrites is described by curvature parameters that represent the coarsening quantitatively, and ends in droplet-like shapes of the secondary dendrite arms at 577 °C. There, the eutectic valley of α-Al/Mg_2Si is reached, forming initially octahedral Mg_2Si particles preferentially at the bases of the secondary dendrite arms. The eutectic grows with seaweed-like Mg_2Si structures, with increasing connectivity. During this solidification stage Fe-aluminides form and expand as thin objects within the interdendritic liquid. Finally, the remaining liquid freezes as ternary α-Al/Mg_2Si/Si eutectic at 558 °C, increasing further the connectivity of the intermetallic phases. The frozen alloy consists of four phases exhibiting morphologies characteristic of their mode of solidification: α-Al dendrites, eutectic α-Al/Mg_2Si "Chinese script" with Fe-aluminides, and interpenetrating α-Al/Mg_2Si/Si ternary eutectic.

Keywords: In situ; Eutectic solidification; Synchrotron radiation computed tomography; 3-D characterization; Cast Al–Mg–Si alloys

1. Introduction

Cast AlMgSi alloys are potential candidates for use in the automotive and aerospace industries [1]. These alloys usually contain α-Al dendrites, primary Mg_2Si particles, α-Al/Mg_2Si eutectic and aluminides originating from Fe and Mn impurities [2]. A ternary eutectic formed by α-Al/Mg_2Si/Si is added to the existing phases as an additional solidification step in case of Si surplus to the stoichiometric Mg:Si ratio (1.74:1) [2,3].

The solidification process during casting determines the microstructure, which is in turn directly linked to the resulting mechanical properties of the alloy. Thus, the morphology of the Mg_2Si phase is strongly dependent on the cooling rate during casting: low cooling rates result in a coarse structure, while fine microstructures can be achieved with higher cooling rates. The primary Mg_2Si particles can have a dendritic or octahedral shape, while the eutectic particles appear with a so-called "Chinese script" shape in two-dimensional (2-D) sections [4,5]. Three-dimensional (3-D) investigations show that the eutectic Mg_2Si phase forms an interconnected coral-like structure [4,6]. The investigation of the kinetics of solidification is necessary to understand how casting parameters, such as cooling rate and temperature gradient in the melt, affect the development of the internal architecture of alloys and consequently determine their resulting mechanical properties.

The solidification of metals has previously been investigated by ex situ methods. The most common way was to

* Corresponding author. Present address: Magnesium Innovation Centre – MagIC, Helmholtz-Zentrum Geesthacht, Max Planck Straße 1, D-21502 Geesthacht, Germany. Tel.: +49 4152 871974; fax: +49 4152 871909.
E-mail address: domonkos.tolnai@hzg.de (D. Tolnai).
[1] On leave from University of Cambridge, UK.

1359-6454
doi:10.1016/j.actamat.2012.01.024

interrupt the solidification at different temperatures, i.e. at different stages of the microstructure's development, by quenching the sample (e.g. [7–9]). Conventional metallographic investigations can be performed on the quenched samples, and quantitative parameters, such as phase area fraction and parameters of the dendritic structure can be determined. The advantage of this method is that it is relatively simple, but it provides only 2-D information. This information can be extended to 3-D by the application of tomographic methods. X-ray tomography [10] and serial sectioning [11,12] provide the possibility for proper spatial quantification of the microstructure, but as in the case of the ex situ methods, without time–temperature resolution of the solidification process.

The development of synchrotron X-ray imaging [13] allows the solidification process to be followed in situ. For instance, a thin plate-like sample can be used as specimen and radiographs can be taken with short acquisition times during solidification, providing an excellent time resolution, as shown for the case of AlCu10 in Refs. [14,15]. The disadvantage of this method is that it only delivers 2-D information on thin samples.

By rotating the sample during solidification, 3-D tomography can be performed [16]. This requires that the tomographic scan be performed faster than the changes in the microstructure within the resolution range. With this method the whole solidification process can be imaged by cooling down the sample to solid state [17–19]. The application of in situ imaging during solidification allows the evolution of the dendritic structure to be followed and permits spatial characterization of the changes in the microstructural parameters, such as interconnectivity or contiguity of eutectic and intermetallic phases. The aim of this work is to characterize the formation and the evolution of the microstructure of an AlMg4.7Si8 alloy by in situ synchrotron tomography during solidification.

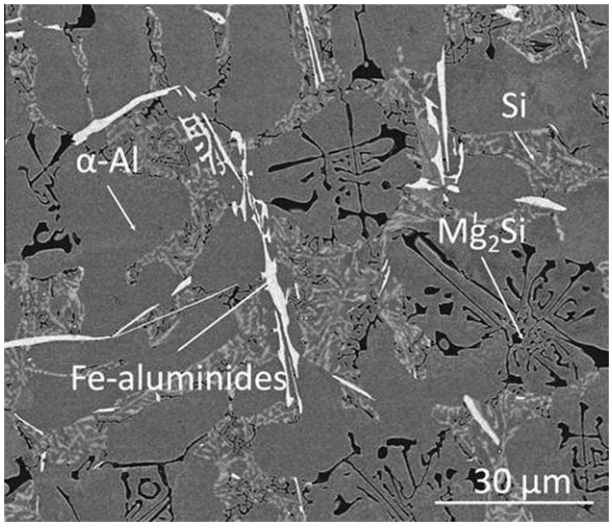

Fig. 1. Backscatter scanning electron image of the investigated material with phases identified by energy dispersive spectroscopy.

2. Experimental methods

2.1. Material

A laboratory gravity cast AlMg4.7Si8 alloy was studied. The Mg:Si ratio in this alloy is 0.58:1, which is lower than the Mg_2Si stoichiometric ratio (1.74:1) [2,3]. The microstructure of the alloy was previously investigated by conventional metallography [3] and ex situ synchrotron tomography [3,6]. It contains four microstructural phases: α-Al dendrites, α-Al/Mg_2Si eutectic, α-Al/Mg_2Si/Si ternary eutectic and Fe-aluminides originating from Fe impurities (~0.5 wt.%). The microstructure of the alloy is shown in a backscattered electron micrograph in Fig. 1 with the phases indicated. Cylindrical specimens 10 mm long and 1.5 mm in diameter were used for the in situ solidification experiments.

2.2. Tomography

The tomography experiment was carried out at the ID15A beamline of the ESRF [20]. A pink beam provided by an U22 undulator was used [21]. 800 Projections were taken between 0° and 180° using an acquisition time of 18 ms per projection resulting in a total scanning time of ~15 s for a complete tomogram. The reconstructions resulted in volumes of 1024^3 voxel with a voxel size of $(1.4\ \mu m)^3$. The furnace to melt the sample comprised two heaters inside a cubic chamber with

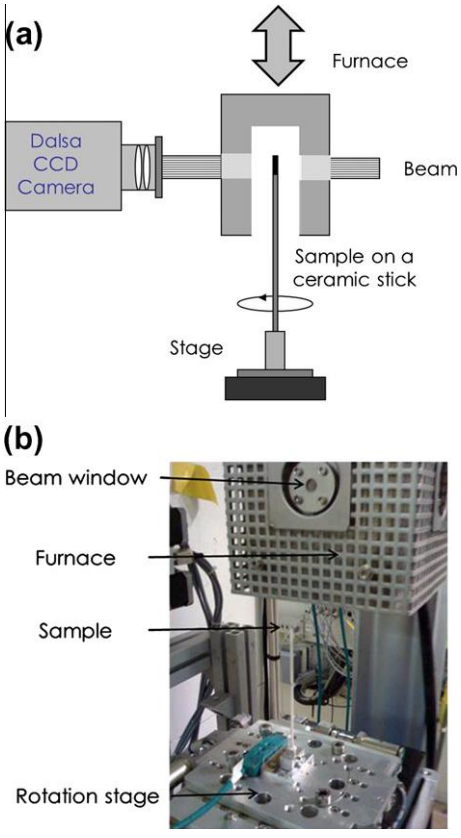

Fig. 2. (a) Schematic representation and (b) picture of the experimental set-up for in situ synchrotron tomography during solidification.

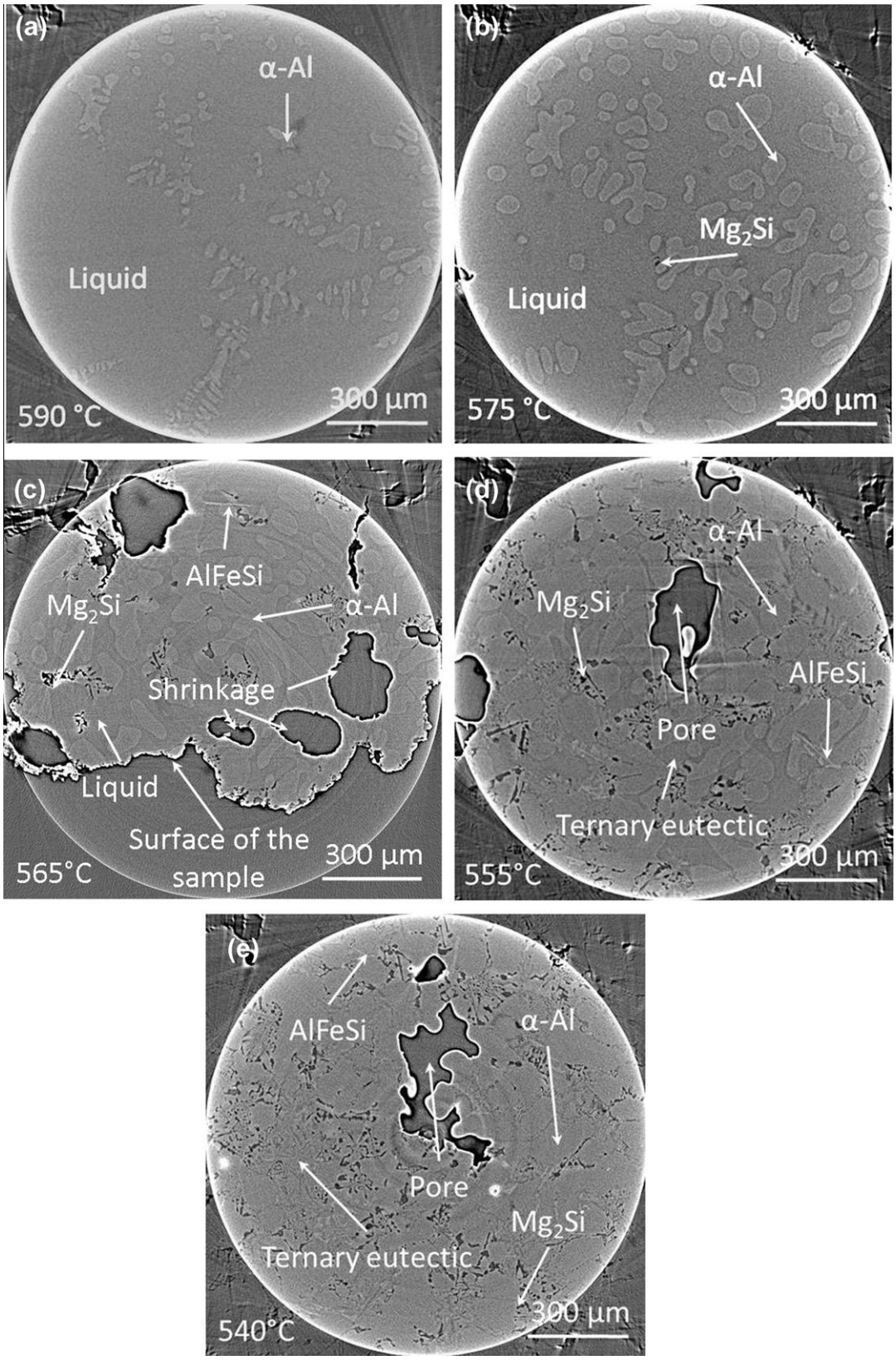

Fig. 3. Reconstructed tomographic slices obtained during in situ solidification of AlMg4.7Si8 at the temperatures at which consecutive solidification of the different phases is observed.

a hole in the bottom through which the specimen can be inserted (Fig. 2). Two windows for the X-ray beam are located on the sides of the furnace chamber. The sample was glued onto a ceramic stick. The molten sample was held by its

own oxide skin during the experiment. The temperature was measured by a thermocouple at the top of the sample. The cooling rate was 5 K min^{-1}, so that the temperature changed by less than 1.5 K during each tomographic scan, which were carried out every minute.

2.3. Image processing

The reconstructed volumes were subjected to a 2-D Gaussian filtering [22] using a mask with a radius of 2 pixels. The 32 bit datasets were converted into 8 bit within the histogram limits −1.5 and 1.5. Registered sub-volumes with a size of $540 \times 400 \times 190$ voxels (0.11 mm^3) were used to analyze the Mg_2Si. This phase was segmented by global thresholding and applying a region-growing algorithm which takes into account the variation of the grey levels in the local environment of the phase considered (a detailed description of the algorithm is given in Ref. [23]). A morphological smoothing was then applied: voxels outside the segmented region having four or more touching neighbours were added to the segmented phase, while voxels belonging to the segmented region and having only one touching neighbour were removed. Only particles larger than 27 voxels (>74 μm^3) were considered for evaluation.

The α-Al dendritic structure was segmented by hand into sub-volumes of $350 \times 220 \times 200$ voxels (0.4 mm^3), which had been previously filtered by a 2-D anisotropic diffusion filter [24] to improve the quality of the reconstructed slices.

Although the qualitative and quantitative results presented in this work are strongly sensitive to the accuracy of the segmentation procedure, the investigations are focused on relative changes during the evolution of the microstructure. Therefore, the results can be considered in relative terms between successive 3-D images treated in the same way.

2.4. Morphological parameters

Morphological parameters have been calculated in order to quantify the changes in the microstructure during the solidification process.

2.4.1. Interconnectivity

In this study the interconnectivity is defined as the relative volume fraction of the largest individual particle (particle = continuous 3-D region of the corresponding phase) of the investigated phase with respect to its total volume fraction in the analyzed volume.

2.4.2. Curvatures

The mean (K) and Gauss curvatures (H), defined as the mean and the product of the principal curvatures, have been determined for the α-Al dendrites during solidification

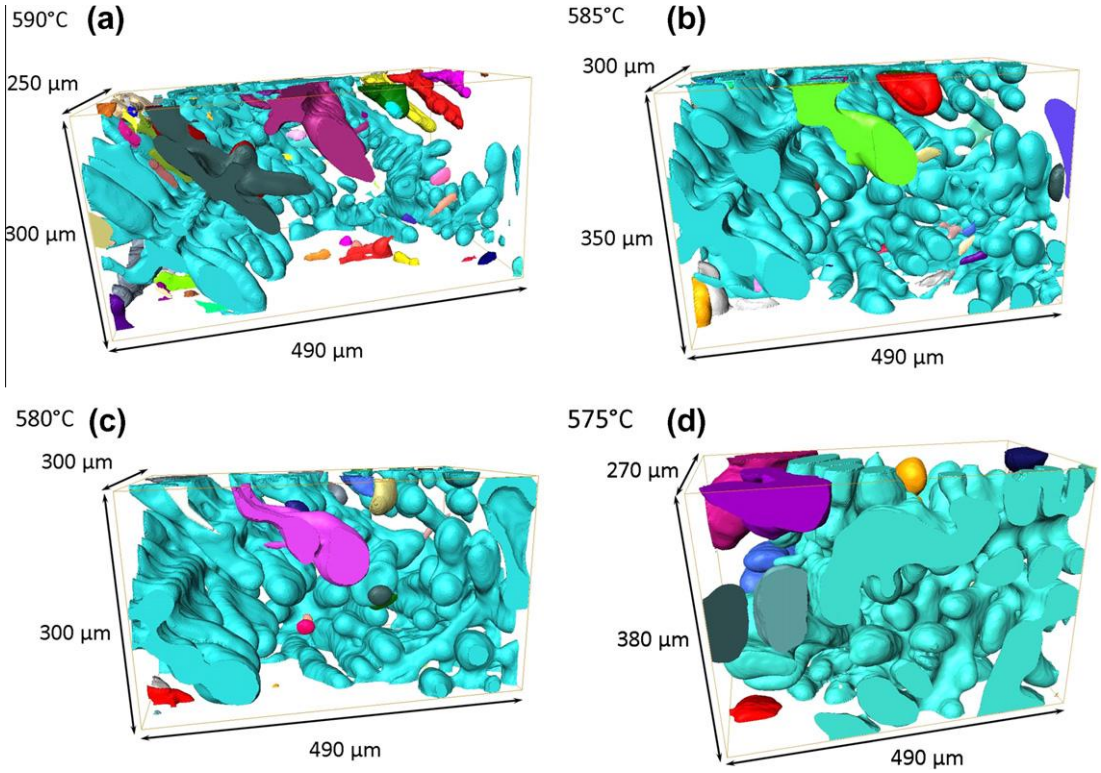

Fig. 4. Growth of the α-Al dendrites in approximately the same region of AlMg4.7Si8 at different temperatures during cooling. The voxel size is $(1.4\ \mu m)^3$. The different colours correspond to different α-Al dendrites within the considered volumes. (For interpretation of the references to colour in this figure legend, the reader is referred to the web version of this article.)

using the Avizo® software [25]. A surface of the voxel-based volume of the segmented phase was produced by a triangular approximation prior to the calculation. The osculant curves have been determined for each triangle of the rendered surface taking into account the neighbouring triangles up to the fifth order. The local radii of these curves were averaged five times with the radii of direct neighbour triangles before the reciprocal of the local radius was calculated. Surfaces which exhibit zero values for the mean and Gauss curvatures simultaneously were excluded from further evaluation in order to avoid phases cut by the borders of the region of interest.

2.5. Differential scanning calorimetry

Calorimetric investigations were performed during cooling at 5 K min^{-1} from 630 to 530 °C with a Perkin-Elmer power-compensated differential scanning calorimeter to analyze the solidification process of the materials. A high-purity Al (99.99 wt.%) sample was used as reference.

3. Results

3.1. In situ synchrotron tomography during solidification

Reconstructed tomographic slices extracted from the in situ solidification experiment of the AlMg4.7Si8 alloy are shown in Fig. 3. The slices show the characteristic temperatures where the phases were first observed during solidification. The α-Al dendrites are resolved for the first time during the experiment at a measured temperature of ~590 °C followed by the α-Al/Mg_2Si eutectic at ~575 °C. Regarding the location where soldification starts: the physical size of the sample (1.5 mm diameter) is larger than the field of view of the radiographies (~1.4 × 1.4 mm^2), and therefore the oxide skin is not visible in Fig. 3a (590 °C). However, looking at the reconstructed slices, one can observe that the dendrites are growing from the outside to the inside, suggesting that the solidification of the dendrites is initiated by the oxide skin of the sample, impeding thus their sinking in the liquid [17]. The Fe aluminides start to grow at ~565 °C. There, the liquid–solid shrinkage produces pores. The last step of the solidification sequence is the formation of the ternary α-Al/Mg_2Si/Si eutectic at

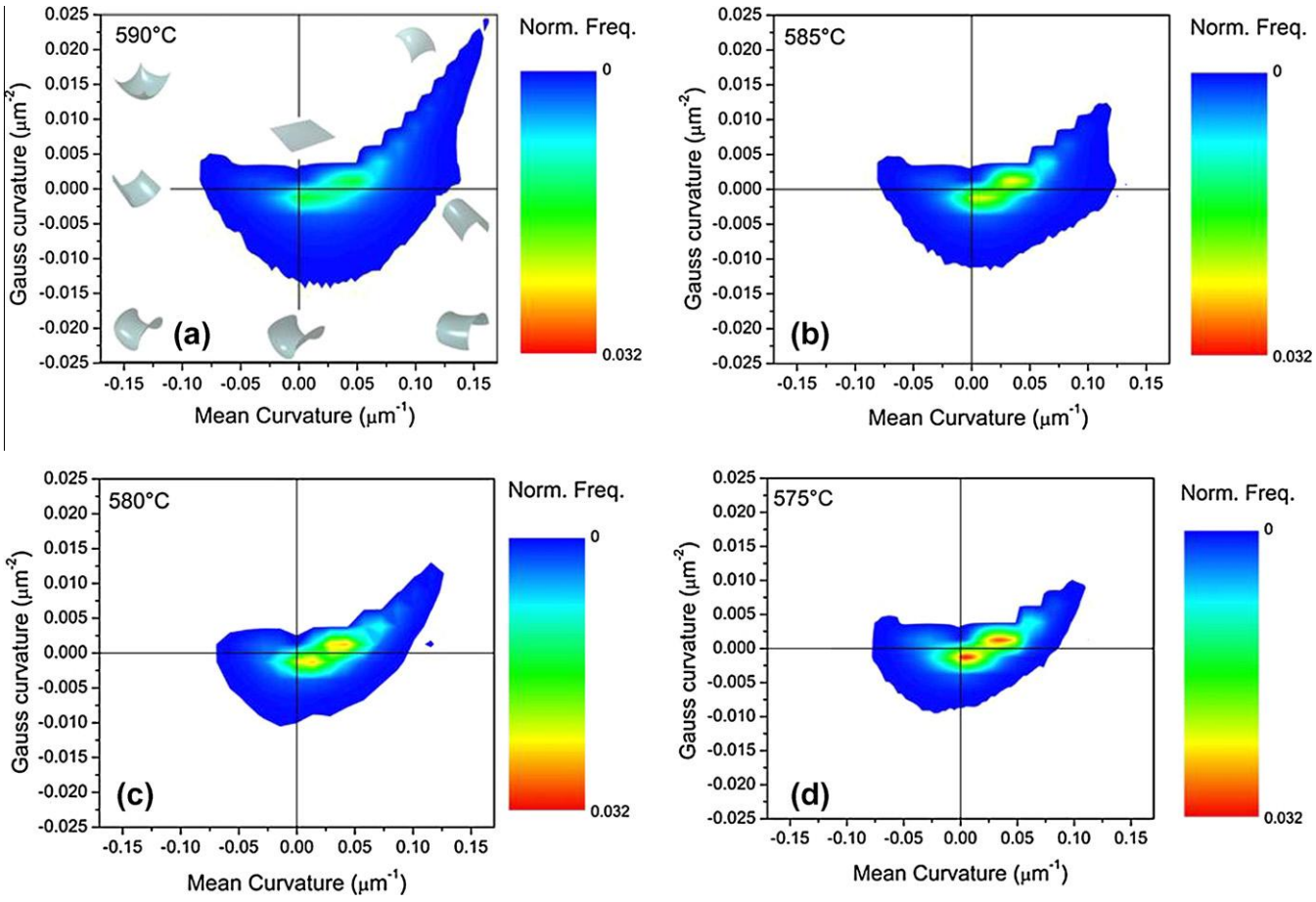

Fig. 5. Curvature distribution of the α-Al dendrites in AlMg4.7Si8 at different temperatures during solidification; correlated characteristic morphologies of surfaces are indicated in the first diagram.

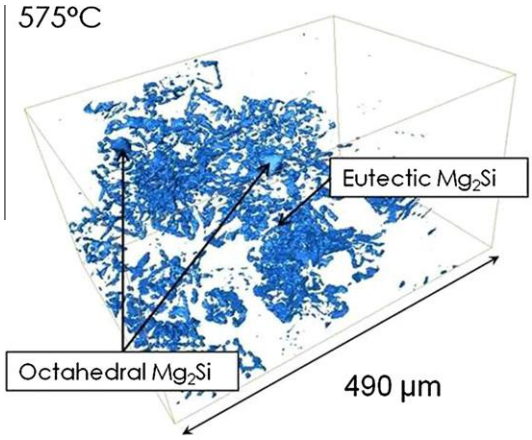

Fig. 6. Mg_2Si particles segmented from microtomography at the onset of their growth at 575 °C.

~555 °C. The slice at 540 °C shows the completely solidified 2-D microstructure.

Rendered 3-D images of the α-Al dendritic solidification at different temperatures during cooling are shown for approximately the same volume in Fig. 4. The smaller secondary dendrite arms tend to disappear, while the larger ones grow, resulting in a coarsening of the dendritic structure during cooling. The growth is asymmetric, with the top of the secondary arms growing faster than the bases. This results in a droplet-like shape and a coalescence of the tops of the secondary dendrite arms.

The distribution of mean and Gauss curvature of the surface of the α-Al dendritic structure at different stages (temperatures) of the solidification process is shown in Fig. 5. The characteristic morphologies for the axes and for each quadrant are indicated schematically in Fig. 5a.

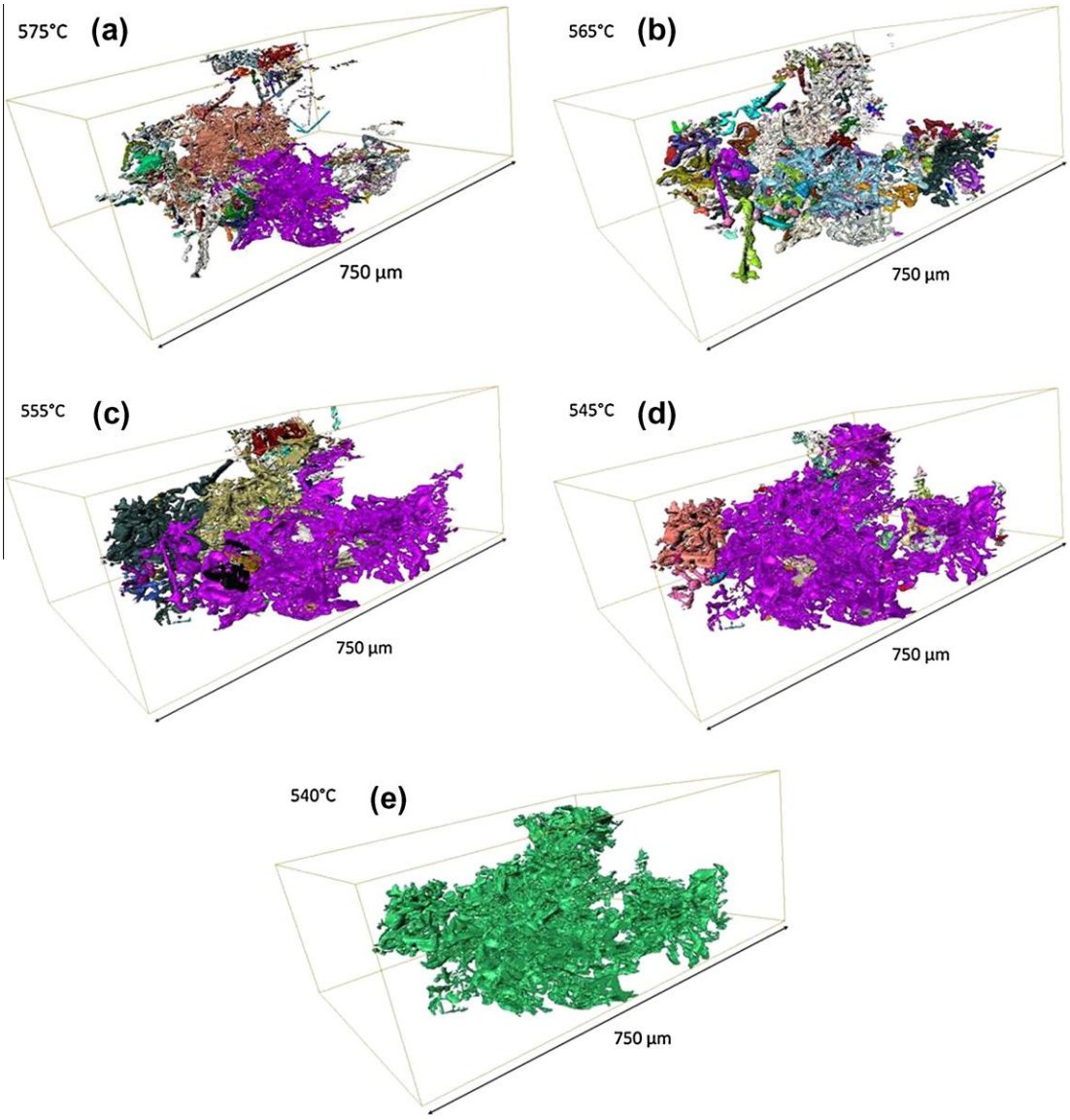

Fig. 7. Mg_2Si particles segmented from the same volume of microtomographies at the indicated temperatures, revealing the evolution of the interconnectivity of the eutectic Mg_2Si particles in AlMg4.7Si8 during solidification. The different colours indicate unconnected particles within the volumes.

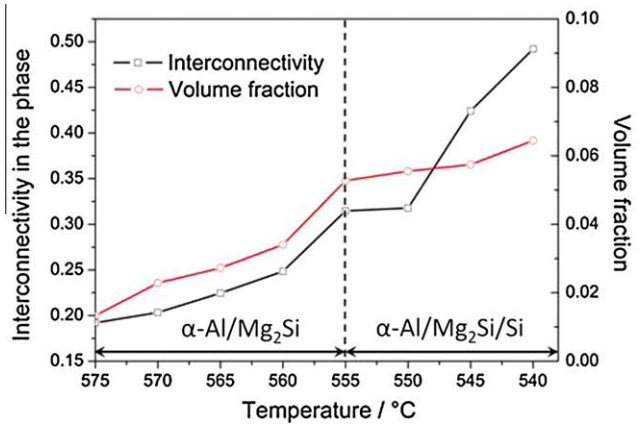

Fig. 8. The evolution of volume fraction and interconnectivity in the eutectic Mg_2Si.

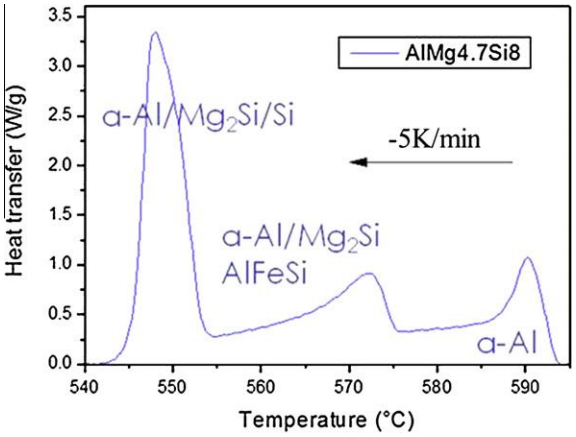

Fig. 9. DSC thermogram during solidification of the AlMg4.7Si8 alloy.

A tail extending to high curvature values can be observed in the positive–positive quadrant of the coordinate system at the onset of solidification. This tail, which indicates the presence of spheroid-like regions with small radii, tends to disappear as the solidification advances. Two maxima of the distribution appear—one close to the origin (flat shape), and one in the positive–positive quadrant (spheroid-like shape)—and both increase in frequency during solidification.

One rendered 3-D volume of the Mg_2Si phase is shown in Fig. 6 at the temperature at which the solidification of the phase was first observed, i.e. ~575 °C. The primary particles present an octahedral shape, while the eutectic structure is seaweed-like. Branches of this structure thicker than 5 μm are resolved. The growth and coalescence of Mg_2Si particles during solidification in the same volume is shown in Fig. 7. The different colours indicate unconnected particles within the investigated volume. At 575 °C (Fig. 7a) several particles are present in the volume; these coalesce during cooling (Fig. 7b–d) and finally join into one interconnected particle as shown in the volume at 540 °C (Fig. 7e). The evolution of interconnectivity and the volume fraction of the Mg_2Si phase are shown in Fig. 8 for a volume of $750 \times 350 \times 265\ \mu m^3$. The interconnectivity at the temperature where the Mg_2Si phase was first observed, namely 575 °C, is 0.19 and shows a monotonic growth until 0.49 at the end of the solidification at 540 °C. The volume fraction of the phase is 1.3% at 575 °C and grows up to 6.4% at the end of the solidification process, counting only particles with diameters >4.2 μm.

3.2. DSC results

The DSC thermogram obtained during cooling from the liquid state at the same rate as in the in situ tomography experiments is shown in Fig. 9. The solidification of the AlMg4.7Si8 alloy starts at ~594 °C with the solidification of the α-Al dendrites. This is followed by an exothermal peak which starts at ~575 °C and reaches its maximum at ~572 °C. The exothermal heat evolution decreases steadily until a third solidification peak starts at ~555 °C. This third peak presents an asymmetric shape that may be an indication of overlapping solidification peaks. The solidus temperature of the alloy is at ~541 °C at the given cooling rate.

4. Discussion

4.1. Solidification sequence

The solidification sequence of the AlMg4.7Si8 alloy at a cooling rate of 5 K min^{-1} can be determined by correlating the results obtained from in situ synchrotron tomography and DSC. The latter technique gives a more accurate temperature measurement, while identification of the individual phases can be performed unequivocally by in situ tomography by reference to the phase diagram. Fig. 10 presents the liquid–solid phase limits for thermodynamic equilibrium according to Thermocalc [3] without considering the Fe content. There, the solidification of the α-Al dendrites starts at $T_m = 591$ °C, reaching the eutectic valley at $T_{eut} = 577.5$ °C, where Mg_2Si continuously solidifies until 558 °C, where the remaining liquid freezes as a ternary

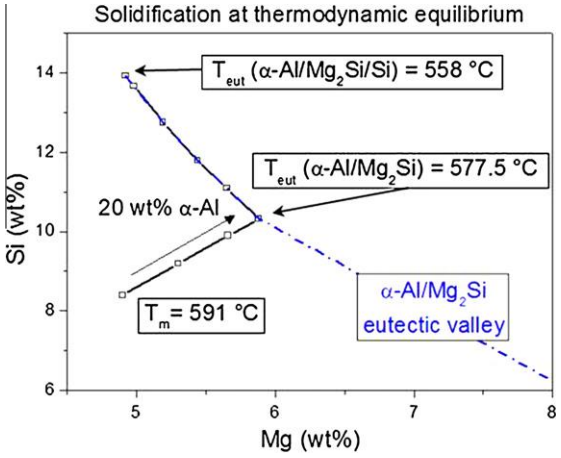

Fig. 10. Thermocalc simulation of the solidification of AlMg4.7Si8 [3].

α-Al/Mg_2Si/Si eutectic. The solidification sequence can be summarized as follows:

α-Al dendrites (594–575 °C) → α-Al/Mg_2Si eutectic(575–555 °C)
→ onset of Fe aluminides at 565 °C
→ α-ternary Al/Mg_2Si/Si eutectic (555–541 °C).

The solidification intervals obtained by both experimental techniques in Table 1 agree reasonably well with the equilibrium conditions calculated by Thermocalc [3], although the experiments were carried out with a finite cooling rate. The asymmetric shape of the first two solidification peaks 594–575 °C and 575–555 °C in the DSC

Table 1
Temperatures of onset of phase solidification in AlMg4.7Si8.

Phases	Calorimetry (°C), cooling rate 5 K min^{-1}	In situ tomography (°C), cooling rate 5 K min^{-1}	Thermocalc (°C) equilibrium
α-Al	594–575	590–575	591
α-Al/Mg_2Si	575–555	575–555	577.5–558
Fe aluminides	Overlap	Onset at 565	Not considered
α-Al/Mg_2Si/Si	555–541	555–540	558

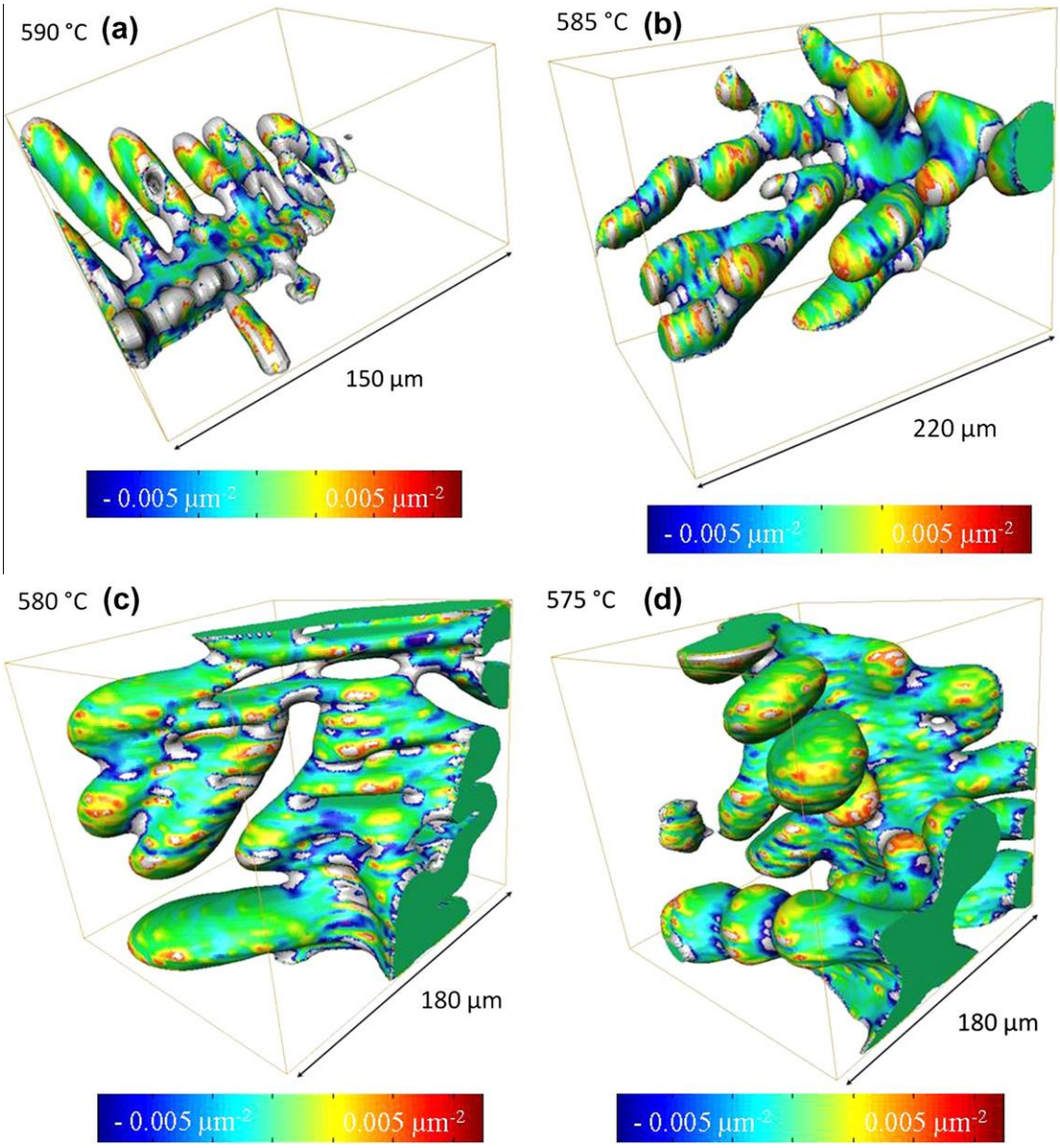

Fig. 11. Typical parts of the dendritic structure during solidification. The colours represent the Gauss curvature between −0.005 and 0.005 μm^2, while the grey parts are outside this range.

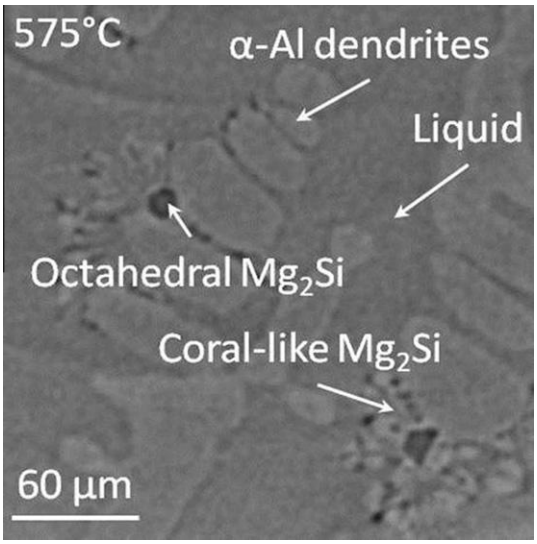

Fig. 12. Tomographic slice recorded at 575 °C showing α-Al dendrites, primary Mg_2Si particles and sections of "Chinese script" Mg_2Si.

thermogram (Fig. 9) are due to the continuous solidification of α-Al and of α-Al/Mg_2Si, respectively. The latter exothermal peak is also extended by the formation of Fe-aluminides. On the other hand, the asymmetry of the last solidification peak (555–540 °C) towards the higher temperature can be understood as an overlap of the almost simultaneous solidification of some Fe-aluminides and the ternary α-Al/Mg_2Si/Si eutectic.

4.2. Dendritic solidification

The change in the morphology of the dendrites during cooling is characterized by coarsening, which is a simultaneous process of growth and coalescence of the secondary dendrite arms, similarly to the case of isothermal coarsening [12]. This can be followed qualitatively on the reconstructed tomographic slices and the rendered volumes shown in Figs. 3 and 4, respectively. As the solidification advances, the growth of the secondary dendritic arms becomes asymmetric, and the tips grow with a higher rate than the bases, resulting in a droplet-like shape, where the tips of neighbouring arms can coalesce [12,26]. This evolution can be followed quantitatively on the curvature distributions (Fig. 5). It should be noted that the dendritic structure in Fig. 4a (590 °C) shows already grown dendrites with secondary arms growing from some primary dendritic arms. This indicates that the very beginning of solidification, where the primary dendrites form, was missed during the experiment. This is due to two reasons: the relatively coarse resolution used (roughly estimated as $\sim 3 \times$ voxel size $\sim 3 \times (1.4\ \mu m)^3$) which limits the possibility of resolving smaller structures; and the fact that scans were carried out every minute, resulting of a "blind" time of up to 60 s during which no tomographic images were taken.

Parts of the dendritic structure during solidification are shown in Fig. 11. The colours represent the Gauss curvature between -0.005 and $0.005\ \mu m^2$, while the grey parts are outside this range. It can be seen that two maxima emerge from the curvature distributions during solidification (Fig. 5): one closer to the origin representing slightly saddle-like phases which are related to the bases and sides of the secondary dendritic arms, and another in the positive–positive quadrant representing spheroid-like regions due to the secondary dendrite tips.

The temperature at which a continuous skeletal dendritic network builds up, known as the dendritic coherence temperature [27], can be estimated between 580 and 575 °C based on the tomographies. Below this temperature the overall macroscopic dimension of the structure remains, except where shrinkage contracts the outer surface; however, shrinkage of the liquid also occurs within the interdendritic spaces, resulting in the formation of porosity.

4.3. Solidification of eutectic Mg_2Si

The location of the onset of the solidification of the Mg_2Si phase can be linked to the bases of the secondary dendrite arms in the interdendritic space as shown in Fig. 12. The solidification of this phase starts with the octahedral shaped particles, from which the seaweed-like eutectic Mg_2Si structure grows [3,6,28].

Several nucleation sites can be observed on the tomographies during solidification, implying that the solidification starts with individually unconnected Mg_2Si structures, which then coalesce as the solidification advances. The ternary eutectic Mg_2Si particles also contribute to the coalescence. Finally, the phase forms a long-range interconnected 3-D structure like that usually found in as-cast conditions (Fig. 7) [6,28].

5. Conclusions

The solidification of an AlMg4.7Si8 alloy has been followed in situ by fast synchrotron microtomography. The following conclusions can be drawn from the results obtained:

- The α-Al dendritic structure coarsens during solidification as a result of the coalescence and growth of the secondary dendrite arms. As the cooling proceeds, the growth becomes asymmetric with the tips of the secondary dendritic arms growing faster than the bases, resulting in a drop-like shape.
- The dendritic coherency temperature is between 580 and 575 °C as determined based on the tomographies.
- The nucleation of the Mg_2Si particles can be linked to the base of the secondary dendrite arms. First, octahedral primary Mg_2Si particles start to solidify at several nucleation sites, followed by the seaweed-like eutectic solidification. The initially separated Mg_2Si particles grow during cooling and finally coalesce to form the long-range interconnected structure observed in the as-cast condition.

- The exact solidification sequence at a cooling rate of 5 K min^{-1} can be determined unequivocally by combining in situ synchrotron tomography and DSC:

α-Al dendrites (594–575 °C) → α-Al/Mg_2Si eutectic (575–555 °C) → Fe aluminides (onset at 565 °C, determined from the in situ tomographic test) → α-Al/Mg_2Si/Si ternary eutectic (555–541 °C).

Acknowledgements

The authors would like to thank the European Synchrotron Radiation Facility for the provision of beam time in the framework of the Long Term Project MA560. P.T. would like to thank the Worshipful Company of Armourers and Braziers for their financial support. D.T., G.R. and H.P.D. are grateful to the Austrian Science Fund (L588-N14, P22876-N22), and D.T. and J.L. as well to the Hungarian Research Fund (OTKA-K-67692).

References

[1] Ostermann F. Anwendungstechnologie aluminium. Berlin: Springer Verlag; 2007.
[2] Mondolfo LF. Al alloys: structures and properties. London: Butterworth; 1976.
[3] Degischer HP, Knoblich H, Knoblich J, Maire E, Salvo L, Suéry M. In: Sonderband d. Praktischen Metallographie, vol. 38; 2006. p. 67–74.
[4] Li C, Wu Y, Li H, Liu XF. Acta Mater 2011;59:1058–67.
[5] Li C, Wu Y, Liu X. J Alloys Compd 2009;477:212–6.
[6] Tolnai D, Degischer HP, Lendvai J. Phys Status Solidi A 2009;8:1850–4.
[7] Liu YL, Kang SB. J Mater Sci 1997;32:1443–7.
[8] Jones H. Mater Sci Eng, A 2005;413–414:165–73.
[9] Iqbal N, van Dijk NH, Offerman SE, Moret MP, Katgerman L, Kearley GJ. J Non-Cryst Solids 2007;353:3640–3.
[10] Fleberbaum M, Rappaz M. Acta Mater 2011;59:6849–60.
[11] Fife JL, Voorhees PW. Acta Mater 2009;57:2418–28.
[12] Mendoza R, Alkemper J, Voorhees PW. Metall Mater Trans A 2003;34A:481–9.
[13] Labiche JC, Mathon O, Pascarelli S, Newton MA, Ferre GG, Curfs C, et al. Rev Sci Instrum 2007;78(9) [art. no. 091301].
[14] Mathiesen RH, Arnberg L, Mo F, Weitkamp T, Snigirev A. Phys Rev Lett 1999;83:562–5.
[15] Mathiesen RH, Arnberg L, Ramsøskar K, Weitkamp T, Rau C, Snigirev A. Metall Mater Trans B 2002;33:613–23.
[16] Ludwig O, Di Michiel M, Salvo L, Suéry M, Falus P. Mater Trans A 2005;36:1515–23.
[17] Limodin N, Salvo L, Boller E, Suéry M, Felberbaum M, Gailliégue S, et al. Acta Mater 2009;57:2300–10.
[18] Terzi S, Boller E, Salvo L, Suéry M. Int J Cast Met Res 2009;22:275–8.
[19] Terzi S, Taylor JA, Cho YH, Salvo L, Suéry M, Boller E, et al. Acta Mater 2010;58:5370–80.
[20] European synchrotron radiation facility. <http://esrf.fr>.
[21] ESRF ID15/A. <http://www.esrf.eu/UsersAndScience/Experiments/StructMaterials/ID15/>.
[22] ImageJ. <http://rsbweb.nih.gov/ij/>.
[23] Tomo3D. <http://metal.elte.hu/tomo3D>.
[24] http://rsbweb.nih.gov/ij/plugins/anisotropic-diffusion-2d.html.
[25] Avizo Fire. <http://vsg3d.com/node/25>.
[26] Mortensen A. Metall Trans A 1989;20(2):247–53.
[27] Claxton RJ. J Met 1975;27:14–6.
[28] Lasagni F, Lasagni A, Holzapfel C, Engstler M, Mücklich F. Pract Metallogr 2010;47:499–587.